Received: Added at production | Revised: Added at production | Accepted: Added at production

DOI: xxx/xxxx

ARTICLE TYPE

Microsecond Nonlinear Model Predictive Control for DC-DC Converters

Aleksandra Lekić[1] | Ben Hermans[2,3] | Nenad Jovičić[4] | Panagiotis Patrinos[5]

[1]Department of Electrical Engineering (ESAT ELECTA), KU Leuven, Leuven, Belgium
[2]MECO Research Team, Department of Mechanical Engineering, KU Leuven, Leuven, Belgium
[3] DMMS lab, Flanders Make, Leuven, Belgium
[4]School of Electrical Engineering, University of Belgrade, Belgrade, Serbia
[5]Department of Electrical Engineering (ESAT STADIUS), KU Leuven, Leuven, Belgium

Correspondence
*Aleksandra Lekić, Email: lekic.aleksandra@kuleuven.be

Summary

In this paper we present a novel nonlinear model predictive control (NMPC) formulation for the transient control of a DC-DC converter. We demonstrate that a real-time implementation of the proposed NMPC scheme using the PANOC solver can be efficiently applied to control DC-DC converters in the microsecond range. Moreover, an embedded, code-generated version of PANOC can be implemented using microcontrollers or digital signal processors. The algorithm is incorporated in the transient simulator of PWM DC-DC converters and the operation of the simulator on the boost converter's example is presented, comparing the performance of our NMPC-controller to that of a classical PID-controller. The operation of the boost converter controlled using the proposed NMPC algorithm is validated experimentally.

KEYWORDS:
DC-DC power converters, Switching Control Systems, Model Predictive Control, Optimal Control.

1 | INTRODUCTION

Switching power converters are circuits used for efficient power conversion[1], with applications in a large variety of electronic devices. Power converters are switching circuits usually controlled using a pulse width modulated (PWM) signal, in which the averaged duration of the PWM logical "1" signal, the so-called duty-ratio, is a scalar in the range of $d \in [0, 1]$. Due to the switching dynamics, the control of power converters is very demanding and complex. For that reason there is a need for better control algorithms[2] and estimation and reduction of the instabilities in the converter[3]. In this work we propose a nonlinear model predictive controller (NMPC) for a specific type of power converters, namely DC-DC converters.

Model predictive control (MPC) has already been applied to control a large variety of circuits[4,5]. The MPC approach for switching linear systems, in which nonlinearity is introduced by switching, has recently been gaining popularity[6,7]. In power electronics, MPC can be applied as an explicit controller through parametric optimization tools [8,9]. Paper[8] illustrates a model predictive controller for a buck converter whose constant switching period is divided into intervals over which the duty-ratio is being fitted. The later work[9] presents explicit MPC for a predefined set of operating regimes. Finite control set MPC has been a topic in[10,11], where it is applied to the power electronics' circuit and compared with a standard linear controller with added modulation. Another approach for the determination of switching in a boost converter is given in[12], where the performance index is obtained as a sum of costs for each operating subsystem.

Recent work related to MPC applied to power converters[13] provides a way for modeling DC-DC converter switching between multiple subsystems as a hybrid system. It is shown that a small prediction horizon in the MPC scheme, which makes the algorithm very fast and real-time implementable, is still sufficient for good control performance[13]. However, the transient overshoot of the state variables during the transient process and after some disturbance in the circuit shows to be rather large[13]. In[14],

a model predictive controller for the output voltage of the pre-compensated discretized DC-DC converter is calculated offline and better performance than the standard voltage mode control (VMC) method is demonstrated. MPC for the reference values of the states of a DC-DC boost converter with a constant switching frequency, has been suggested in [15], where the authors demonstrate that the suggested approach is suitable for real-time implementation for converters with a switching period of $T_S = 50\ \mu$s. Comparing to the work of [15] related to the design of MPC for boost converters, our work is modular and it does not depend on the DC-DC converter's design. Our algorithm is therefore also applicable to converters with multiple switches and reactive elements (like SEPIC or a Ćuk converter). Recent work [16] presents a design of the MPC voltage-mode-controlled boost converter with more degrees of freedom regarding the controller tuning. However, the proposed control [16] for the given boost configuration operating with the switching frequency $f_S = 200$ kHz enables the change of the inputs on a twice lower MPC frequency without on-line optimization, which is the main difference to our work.

On top of their usage in DC-DC converter control, MPC algorithms have also been developed to control power converters integrated with renewable power sources. One such example is MPC constructed to control a DC-DC converter powered by a PV module [17]. Another state-of-the-art problem is the control of the AC-DC and DC-AC converters used for efficient power conversion between wind farms and High Voltage Direct Current (HVDC) grids, and HVDC and AC grids. These converters are usually constructed as two level converters or Modular Multi-terminal Converters (MMCs). Since these converters are new and prominent, and moreover very important for future energy development, the control methods are also being rapidly developed. MPC methods found their application for the control of two level converters [18,19] using finite control set MPC. Similarly, there are efficient algorithms for finite control set MPC for the AC-DC converters as in [20] and for matrix converters [21]. Also, one more application is MPC control for multilevel converters used to improve traction in electric vehicles [22].

In this work we present a controller for DC-DC converters using constrained nonlinear model predictive control [23]. Unlike the previous work where the MPC input and the cost are determined using state variables [13,14,15], in our work MPC is used for the determination of the duty-ratio for the constant frequency DC-DC converter. Our approach has the important advantage of eliminating the need for deciding upon a switching signal, thus avoiding the usage of boolean variables in the resulting optimal control problems. Each resulting optimization problem is shown to be solved in one switching period of 50μs.

The MPC algorithm is automated and incorporated in the simulator of [24]. Thus, the MPC algorithm can automatically be applied to different converter's configurations. The simulator, which can be found in repository [25], gives the possibility of MPC, PID control and open loop simulation of the two switch PWM DC-DC converters. The MPC controller relies on the PANOC algorithm developed in [26], tailored for NMPC problems. PANOC is implemented in the C programming language [23] using the CasADi package [27] for automatic differentiation. NMPC files containing the C code are automatically generated and they can be used for programming the microcontroller or DSP. The implementation of the simulator in a lower level programming language, such as C, makes our algorithm very fast and results in microsecond running times. For the purpose of further speeding up the NMPC convergence, like in [14,15], the NMPC horizon was drastically decreased, even to the value $N = 2$, and still provides sufficiently good transient performance with a small overshoot. For the high speed experimental implementations the algorithm can be parallelised and implemented on FPGA or in ASIC.

The paper is organized as follows. Section II presents the optimal control problem for switching DC-DC converters and a discussion on the algorithmic aspects. Section III presents and discusses the simulation results of this algorithm applied to the three commonly used converters: boost, buck and Ćuk converter. In section IV the experimental results for the NMPC of the boost converter are given. Finally, section V draws concluding remarks.

2 | MODEL PREDICTIVE CONTROL OF DC-DC CONVERTERS

During one switching period $T_S = 1/f_S$, where f_S is switching frequency, DC-DC converter switches between subsystems described using ordinary differential equations (ODE). Assuming that in the i-th subsystem, where $i = 0, \dots, Z-1$ and Z is the number of subsystems in the one switching period, in the switching period j converter operates during the time interval $\tau_{i,j} \leq t < \tau_{i+1,j}$, then converters' dynamics can be presented with equation:

$$\dot{x} = f_i(x(t)) = A_i\, x + b_i. \tag{1}$$

Each of the subsystems is presented using ODE (1), where $A_i \in \mathbb{R}^{n\times n}$ is a matrix and $b_i \in \mathbb{R}^n$ is a column vector corresponding to the i-th subsystem and n denotes the number of the state variables.

During one switching period the DC-DC converter can switch between multiple subsystems, but the most desirable operation regime is the so-called continuous conduction mode (CCM). In CCM, the DC-DC converter switches between two subsystems [1],

denoted as subsystem 0 and subsystem 1. Thus, in the remainder of this text we will consider two switching intervals, $\left[\tau_{0,j}, \tau_{1,j}\right]$ and $\left[\tau_{1,j}, \tau_{2,j}\right]$ with $\tau_{0,j} < \tau_{1,j} < \tau_{2,j}$ and $\tau_{0,j} = jT_S$, $\tau_{2,j} = (j+1)\,T_S$ in the j-th switching period.

In CCM converter's equilibrium or the steady-state values of the state variables are determined by applying the Volt-second and Ampere-second balances [1]. The equilibrium is determined for a desired duty-ratio $\overline{d}$ and switching frequency f_S by solving the equation:

$$\overline{x} = \left(\overline{d}A_0 + (1-\overline{d})A_1\right)^{-1} \left(\overline{d}b_0 + (1-\overline{d})b_1\right). \tag{2}$$

This approach is based on averaging and linear perturbations [28]. Perturbations of the state variables are denoted as ripple Δx and they are often calculated using linear ripple approximation (LRA) [1]. LRA stems from the fact that in power electronics circuits the time constants caused by reactive elements are much greater than the switching period and thus, the state variables can be presented as linearly increasing or decreasing during the switching period. Using LRA, the ripple in steady-state in CCM can be determined as

$$\Delta x = \frac{\overline{d}T_S}{2}\left(A_0\overline{x} + b_0\right). \tag{3}$$

In the CCM's steady-state it is assumed that steady-state values at the beginning and at the end of the switching period are equal and that their value is

$$x(\tau_{0,j}) = x(\tau_{2,j}) = \overline{x} - \Delta x, \tag{4}$$

while after operation in the subsystem 0 the state is $x(\tau_{1,j}) = \overline{x} + \Delta x$.

2.1 | MPC formulation

The MPC problem of a DC-DC converter is formulated as a multistage optimal control problem. One switching period is divided in 2 subsystem intervals $\tau_{i,k} \le t < \tau_{i+1,k}$ for $i = 0, 1$, $k \in \{0, \dots, N-1\}$ and prediction horizon N. Then the values $d_k^0 = \frac{\tau_{1,k}-\tau_{0,k}}{T_S}$ and $d_k^1 = \frac{\tau_{2,k}-\tau_{1,k}}{T_S}$ denote the normalized duration of the operation in subsystem 0 and 1 respectively. The values of state variables in the k-th switching period at the beginning and at the end of the operation in the subsystem 0 are x_k and $x_{k+1/2}$, and in subsystem 1 are $x_{k+1/2}$ and x_{k+1}. Then using the equation (1), we can write discrete time dynamics

$$x_{k+1/2} = F_0(x_k, d_k^0), \qquad x_{k+1} = F_1(x_{k+1/2}, d_k^1), \tag{5}$$

where

$$F_i(x, d) = e^{A_i T_s d}x + \int_0^{T_s d} e^{A_i t} b_i \,\mathrm{d}t. \tag{6}$$

In fact we can define

$$F(x, d) = F_1(F_0(x, d), 1-d), \tag{7}$$

where $0 \le d \le 1$. Then the difference equation is:

$$x_{k+1} = F(x_k, d_k), \tag{8}$$

where $d_k = d_k^0$. The problem becomes a standard NMPC problem:

$$\begin{aligned}
\textbf{minimize} \quad & \sum_{k=0}^{N-1} \left(\psi(d_k) + \ell(x_k)\right) + \ell_N(x_N) \\
\textbf{subject to} \quad & x_{k+1} = F(x_k, d_k), && k \in [0, N-1], \\
& 0 \le d_k \le 1, && k \in [0, N-1].
\end{aligned}$$

The stage costs $\psi(d_k)$ and $\ell(x_k)$ are quadratic functions expressing the distance of the duty-ratios and system states to respectively the steady-state duty-ratios and the system state variables' equilibrium and maximum state variables' ripple in the steady-state [1], denoted as $\overline{d}$, $\overline{x}$ and Δx, respectively:

$$\psi(d_k) = R\left(d_k - \overline{d}\right)^2, \tag{9a}$$

$$\ell(x_k) = \left(x_k - \overline{x} + \Delta x\right)^\intercal Q \left(x_k - \overline{x} + \Delta x\right), \tag{9b}$$

$$\ell_N(x_N) = (x_N - \overline{x} + \Delta x)^\intercal P\,(x_N - \overline{x} + \Delta x), \tag{9c}$$

where the scalar $R > 0$ and matrices $Q, P \succ 0$ are positive definite matrices. The difference equation (8) gives values of the state variables at the end of the switching period, which in steady-state have the value of (4). Thus, the state and terminal costs in (9b)-(9c) are determined by the difference of the state values to the steady-state value from equation (4).

2.2 | Numerical aspects

The proposed NMPC problem is solved at every time step using PANOC, a recently introduced optimization algorithm [23,26]. This algorithm combines proximal gradient steps and limited memory BFGS steps to efficiently iterate towards an optimal solution. It can thus deal with an optimization problem consisting of an objective function and a set of easy to project upon constraints. Therefore, the system dynamics have to be eliminated from the problem by substitution, yielding the well known single shooting formulation, in which only the duty ratios remain as decision variables.

To generate the solution iterates, PANOC requires the Jacobian of the objective function, and thus of the dynamics, with respect to the state and input. The Jacobians of the dynamics can be calculated analytically, as is shown below.

Recall that, from (7), the system dynamics are given as a succession of two functions, F_0 and F_1. These can be rewritten using equation (6), as $F_i(x,d) = f_1^i(x,d) + f_2^i(d)$, with

$$f_1^i(x,d) = e^{AT_s d}x, \text{ and } f_2^i(d) = \int_0^{T_S d} e^{A_i t} b_i \,\mathrm{d}t.$$

Note that this system is linear with respect to the state x and nonlinear with respect to the control input d. We have

$$\frac{\partial f_1^i}{\partial x}(x,d) = e^{A_i T_s d}, \quad \frac{\partial f_1^i}{\partial d}(x,d) = T_S A_i e^{A_i T_S d} x,$$
$$\frac{\partial f_2^i}{\partial d}(d) = T_S e^{A_i T_S d} b_i,$$

where we made use of Leibniz's rule[1].

Therefore, in order to compute the next state and the Jacobians we only need to calculate $e^{A_i T_S d}$. Since A_i are constant matrices, we can compute the Jordan decomposition of A_i offline, $A_i = P_i J_i P_i^{-1}$, where J_i is (block) diagonal. Then, evaluating $e^{A_i T_S d}$ for different values of d requires only $O(n^2)$ operations, using

$$e^{A_i T_s d} = P_i e^{J_i T_S d} P_i^{-1}.$$

In fact, if A_i is diagonalizable, which is valid for almost all switching converters and therefore we may assume for simplicity, matrix J_i can be chosen to be diagonal and then

$$e^{A_i T_S d} = P_i \mathrm{diag}(e^{\lambda_k T_S d}) P_i^{-1}.$$

2.3 | MPC Stability

Showing that the designed MPC controller is stable for this circuit is a complicated procedure, as it involves a nonlinear system, and we cannot explicitly enforce a terminal constraint on the state. According to sections 2.5.5 and 2.6 in [29], however, stability can still be guaranteed for this controller. The design of a stable controller involves two steps, which are briefly outlined below.

Firstly, to deal with the nonlinearity, a globally stabilizing linear controller is first designed for the system linearized around the equilibrium point, given by equations (2), (3) and (4). Linearization around the origin for the given system provides the difference equation

$$y_{k+1} = A_d\, y_k + b_d\, r_k, \tag{10}$$

[1] Leibniz's rule:

$$\frac{\mathrm{d}}{\mathrm{d}d}\int_{a(d)}^{b(d)} g(d,t)\mathrm{d}t = g(d,b(d))\frac{\mathrm{d}}{\mathrm{d}d}b(d) - g(d,a(d))\frac{\mathrm{d}}{\mathrm{d}d}a(d)$$
$$+\int_{a(d)}^{b(d)} \frac{\mathrm{d}}{\mathrm{d}d} g(d,t)\mathrm{d}t$$

where $y_k = x_k - \overline{x} + \Delta x + A_d^{-1} c_d$ and $r_k = d_k - \overline{d}$. The matrix A_d and the vector b_d are obtained as the Jacobians around the origin: $A_d = F_x(\overline{x} - \Delta x, \overline{d})$ and $b_d = F_d(\overline{x} - \Delta x, \overline{d})$, while and the vector $c_d = F(\overline{x} - \Delta x, \overline{d})$. With the objective function as a Lyapunov function, a globally stable linear controller $r = Ky$ for this linear system and the appropriate terminal penalty matrix P can be found from the well known Ricatti equation:

$$\begin{aligned} K &= -(b_d^\intercal P b_d + R)^{-1} b_d^\intercal P A_d, \\ P &= (A_d + b_d K)^\intercal P (A_d + b_d K) + 2Q. \end{aligned} \tag{11}$$

The stability of the controller can then also be guaranteed for the nonlinear system locally around the linearization point, by quantifying the nonlinearity of the dynamics and enforcing a terminal constraint as a sublevel set of the Lyapunov function.

Secondly, to compensate for the lack of an enforced terminal constraint, the terminal penalty is multiplied by a factor β. This guarantees stability for a set of initial states, also known as the region of attraction. Specifying that this region of attraction contains all normal operating points then guarantees stability of the MPC controller for the nonlinear system. This, and the subsequent extraction of the value for β, however, is difficult in practice and leads to conservative results. In this paper, β is chosen to be equal to 1, and convergence to the equilibrium point is verified in the simulations.

According to[29], in order to show the system's stability for the linearized model around the origin as in equation (10), we have to choose control $r = Ky$ such that $A_K = A_d + b_d K$ is stable, meaning that all eigenvalues of A_K are inside the unit circle. An unconstrained MPC problem for nonlinear systems is stable under a Lyapunov function defined as[29]:

$$V(y) = \ell_N(y) + \sum_{j=0}^{N-1} \ell(y(j), r(j)) = |y|_P^2 + \sum_{j=0}^{N-1} (|y(j)|_Q^2 + |r(j)|_R^2), \tag{12}$$

where $|y|_X^2 = y^\intercal X y$ for a square matrix X. The following property then needs to be satisfied:

$$\begin{aligned} &\ell_N(f(y, Ky)) - \ell_N(y) + \ell(y, Ky) \leq 0, \\ &\Rightarrow \ell_N(A_K y) - \ell_N(y) + \ell(y, Ky) \leq 0, \\ &\quad |A_K y|_P^2 - |y|_P^2 + |y|_Q^2 + |y|_R^2 \leq 0. \end{aligned} \tag{13}$$

The inequality (13) provides the condition

$$y^\intercal (A_K^\intercal P A_K - P + Q + K^\intercal R K) y \leq 0. \tag{14}$$

A way to solve previous problem (14) is to solve following equations[30]:

$$A_d^\intercal P A_d - P + Q + K^\intercal (b_d^\intercal P b_d + R) K + K^\intercal b_d^\intercal P A_d + A_d^\intercal P b_d K = 0,$$

which can be solved as a Riccati equation under assumption that

$$K = -(b_d^\intercal P b_d + R)^{-1} b_d^\intercal P A_d, \tag{15}$$

by solving

$$A_d^\intercal P A_d - P + Q - A_d^\intercal P b_d (b_d^\intercal P b_d + R)^{-1} b_d^\intercal P A_d = 0. \tag{16}$$

Equation (14) is sufficient to prove stability of the system using the control Lyapunov function[29], meaning that the Lyapunov function from equation (12) is valid because:

$$\begin{aligned} &\lambda_{\min}(P) ||y||^2 \leq V(y) \leq \lambda_{\max}(P) ||y||^2, \\ &\Delta V(y) \leq -\lambda_{\min}(Q) ||y||^2. \end{aligned}$$

With $\lambda_{\min}$ and $\lambda_{\max}$ we denote minimum and maximum eigenvalue, respectively.

However, in our MPC algorithm, no kind of terminal constraints are enforced. As is done in Section 2.6 in[29], a constraint on the initial state can be recovered as an implicit constraint on the terminal set:

$$Y_f = \{y \in \mathbb{R}^n | \ell_N(y) \leq \alpha\}.$$

Here, $\alpha = (\overline{x} - \Delta x)^\intercal P (\overline{x} - \Delta x)$. The region of the attraction is then given as

$$\Gamma_N = \{y | \hat{V}(y) \leq Ne + \beta\alpha\} \tag{17}$$

with $\hat{V}(y)$ the optimal cost as a function of the initial state, and $e = \lambda_{\min}(P^{-1/2} Q P^{-1/2})$[31]. Note again that we put $\beta = 1$.

2.4 | MPC Program Implementation

The DC-DC simulator is implemented in the Python 3.6 programming language. This program offers an interface which allows choosing the type of the control. As an input file, it takes a netlist of the converter[24].

The simulator generates all possible converter's subsystems first[24]. For every subsystem the system matrices are determined, both in numpy and CasADi[27] format. For the list of possible subsystems are formed possible switching sequences between subsystems. The simulation of DC-DC can be done in open loop, in closed loop with a PID controller discretized using a pole-zero placement method or in closed loop with a NMPC[25].

The simulation of the PWM converter controlled using NMPC takes the generated state-space model and states and forms the NMPC model. Then, the cost function is produced and the controller is generated as it is described in section 2. It must be noted that the controller is generated in C and this code can be used for its implementation on a microcontroller or a DSP[23]. The design of the NMPC is completely automatized and it does not depend on the topology of the chosen DC-DC converter. After generation of the code, the transient simulations starts. After running the simulation, results can be plotted directly in Python using the matplotlib package.

3 | SIMULATIONS

This section presents simulation results for the NMPC controlled DC-DC converter. The proposed NMPC controller will be compared against an open loop boost converter. A boost converter is chosen as a representative, commonly used switching converter, which during his operation switches between marginally stable and stable subsystems.

3.1 | Boost Converter's Simulations

3.1.1 | Operating of the Boost Converter

The boost converter depicted in Figure 1 operates in three subsystems. A PWM signal is used to control the switch S (realized as a transistor, see Figure 1). Subsystem 0 denotes the circuit with switch S turned on and diode D turned off, and is described

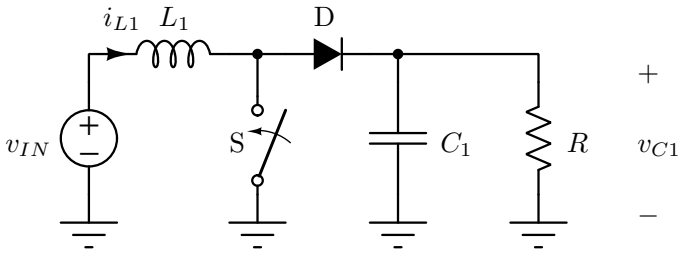


FIGURE 1 Boost converter.

in state-space form using matrices

$$A_0 = \begin{bmatrix} 0 & 0 \\ 0 & -\frac{1}{RC_1} \end{bmatrix}, \qquad b_0 = \begin{bmatrix} \frac{v_{IN}}{L_1} \\ 0 \end{bmatrix}, \tag{18}$$

for the state variables $x = [i_{L1}\ v_{C1}]^T$. Subsystem 0 is marginally stable.

Subsystem 1 denotes the circuit with switch S off and the diode D on, so the system matrices become

$$A_1 = \begin{bmatrix} 0 & -\frac{1}{L_1} \\ \frac{1}{C_1} & -\frac{1}{RC_1} \end{bmatrix}, \qquad b_1 = \begin{bmatrix} \frac{v_{IN}}{L_1} \\ 0 \end{bmatrix}. \tag{19}$$

This subsystem is stable.

Operation between subsystems 0 and 1 presents CCM of the boost converter. The equilibrium states of the boost converter in CCM for a fixed desired duty-ratio $\overline{d}$ are, according to (2), equal to

$$\overline{x} = \left[\overline{i_{L1}}\ \ \overline{v_{C1}}\right]^\intercal = \left[\frac{v_{IN}}{(1-\overline{d})^2 R}\ \ \frac{v_{IN}}{1-\overline{d}}\right]^\intercal. \tag{20}$$

The boost converter ripple in the steady-state using (3) is given by

$$\Delta x = \left[\frac{v_{IN}}{L_1}\overline{d}T_S \;\; -\frac{\overline{v_C}}{RC_1}\overline{d}T_S\right]^\intercal. \tag{21}$$

3.1.2 | Simulation of the Controlled Boost Converter

An open loop, PID and an NMPC driver are constructed for the boost converter with the following circuit parameters: $v_{IN} = 10$ V, $L_1 = 100$ μH, $C_1 = 20$ μF, $R = 4$ Ω and switch S driven using PWM with a constant frequency $f_S = 50$ kHz and steady-state duty-ratio $\overline{d} = 0.3$. The simulated boost converter has equilibrium calculated using Eq. (20) and it is $\overline{x} = [5.1\text{ A},\ 14.29\text{ V}]^\intercal$. The ripple of the boost converter in CCM is given in Eq. (21), and for this example it is $\Delta x = [0.3\text{ A}, -0.54\text{ V}]^\intercal$. All simulations are performed using the simulator developed in[24] with the incorporated NMPC controller[23].

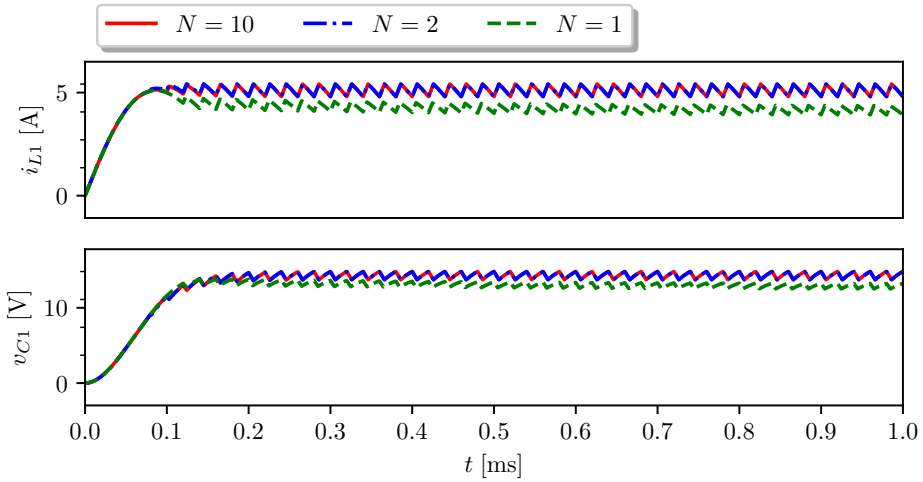


FIGURE 2 Boost converter's transient response with NMPC applied for different prediction horizon values $N \in \{1, 2, 10\}$.

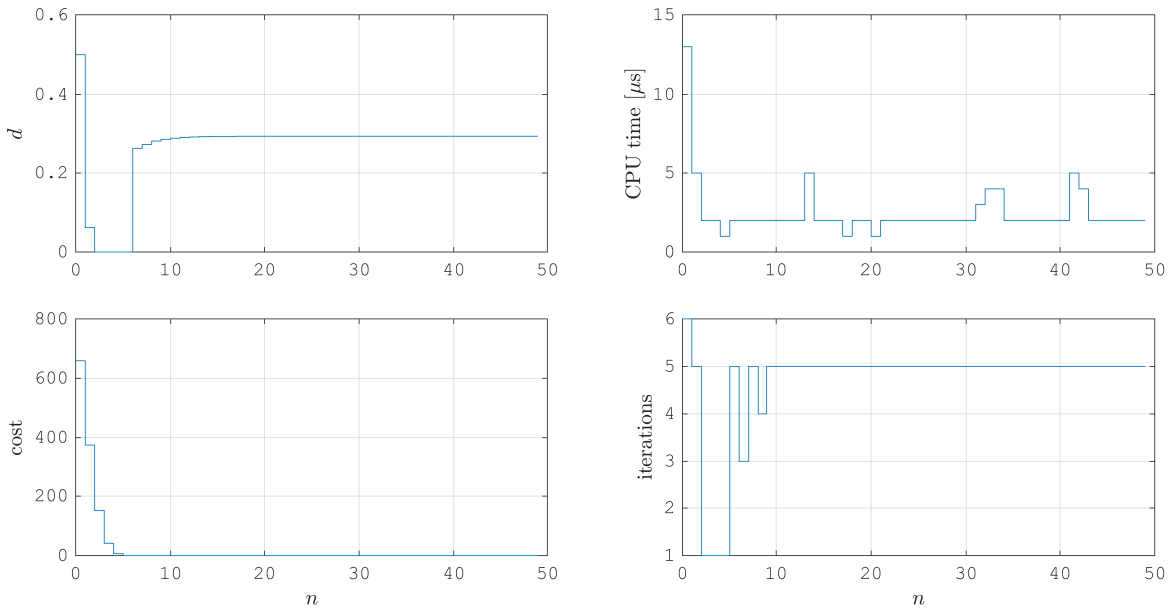


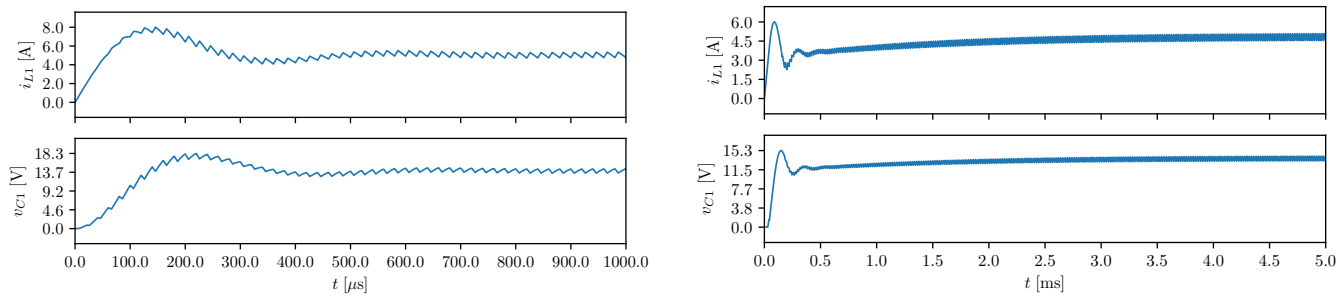
FIGURE 3 Optimal duty ratios, objective function values, CPU times and PANOC iterations for the resulting optimal control problem in NMPC with a horizon $N = 2$.

As described before, NMPC is applied to provide a desired steady-state operation. For the specific example of the boost converter this means that with the provided circuit parameters (values for circuit components) and with a desired switching frequency and duty-ratio in steady-state, NMPC will determine the duration of operation in every subsystem during each switching period, to evolve optimally towards steady-state. The cost function terms (9a)-(9b) are constructed using matrices $Q = I_{2\times 2}$ and $R = 0.1$, and hence the terminal cost matrix is determined as

$$P = \begin{bmatrix} 4.2135 & 1.5124 \\ 1.5124 & 1.7147 \end{bmatrix},$$

using Eq. (16). Figure 2 contains the simulated transient response of the state variables in the boost converter with NMPC applied for the different values of the switching prediction horizon $N \in \{1, 2, 10\}$. From Figure 2 it can be observed that the waveforms of the state variables for the chosen prediction horizon $N = 10$ and $N = 2$ show very similar behavior, while for $N = 1$ the boost converter does not satisfy the requirements for the steady-state operation. Figure 2 clearly shows that the state converges to the equilibrium state. The NMPC controller is thus observed to be stable for the given circuit and operating regime, even if we use $\beta = 1$ in the terminal penalty. A higher terminal penalty is therefore unnecessary and would only lead to a more ill-conditioned problem and slower sampling time.

The transient diagrams of the NMPC boost converter are depicted in Figure 2. Figure 3 presents the obtained values for the optimal duty-ratio, the optimal cost, the number of PANOC iterations and CPU run time for the first 15 switching periods. These simulations were performed on a notebook with Intel(R) Core(TM) i7-8565U CPU @ 1.80GHz x 4 processor and 16 GB of memory. From Figure 3 it can be seen that the cost decreases as converter's system "approaches" its steady-state operation. The CPU time to compute the next set of optimal duty ratios is always smaller than the switching period duration.



(a) (b)

FIGURE 4 Boost converter's transient response: (a) in the open loop; (b) with the applied PID controller.

In order to present the benefits of the NMPC proposed in this paper, the transient diagrams of the state variables of the boost converter operating both in the open loop, controlled using PID controller and controlled using NMPC are provided. In Figure 4a the diagrams of the state variables operating in open loop are depicted. Comparing with the open loop response from Figure 4a, it can be seen that the usage of the proposed algorithm eliminates "overshoot", especially visible in the inductor current plot, and significantly shortens transient time.

The PID controller for the boost converter is designed for the averaged model of the converter using a lead-lag compensator, with the same steady-state reference output voltage. The lead compensator ensures phase margin of 45° at the crossover frequency being $f_C = \frac{f_S}{10}$, whereas the lag compensator eliminates the steady-state error. The transfer function of the PID controller in the Laplace domain is:

$$H_{PID}(s) = \frac{2.829 \cdot 10^{-6} s^2 + 0.02847 s + 61.51}{7.013 \cdot 10^{-6} s^2 + s}.$$

In Figure 4b the transient diagrams of the boost converter controlled using discretized PID controller[24] are presented. It can be seen that the "overshoot" on the state variables is smaller than in open loop, but larger than in NMPC, and the settling time is much longer as well.

Compared to the recent publications[15,16] our NMPC algorithm does not require extensive change of the controller's configuration for different types of the converters. Operating results show to be comparable and easily applicable to the real-time applications using simulation generated C files.

3.1.3 | NMPC with a change of the operating conditions

This subsection describes two examples of the boost converter with the same circuit parameters as given in subsection 3.1.2 and with a constant switching frequency $f_S = 50$ kHz. The first example shows the behavior in the case of a steady-state change during the converter's operation. The second example presents the outcome in the case of a change of input voltage.

Figure 5 present transient diagrams of the state variables for the case of changing the desired operating point. In particular, the desired duty-ratio is $\overline{d} = 0.3$ and thus, the desired steady-state is $\overline{x} = [5.1\text{ A},\ 14.29\text{ V}]^\intercal$. Then, after the first 1 ms the desired operating point is changed to a duty-ratio $\overline{d} = 0.5$ and steady-state $\overline{x} = [10\text{ A},\ 20\text{ V}]^\intercal$. Figure 6 provides results of running the simulation with optimal duty ratios, objective function values, CPU times and PANOC iterations. It can be concluded that even in the case of the change in the operating condition, the CPU time remains lower than the switching period.

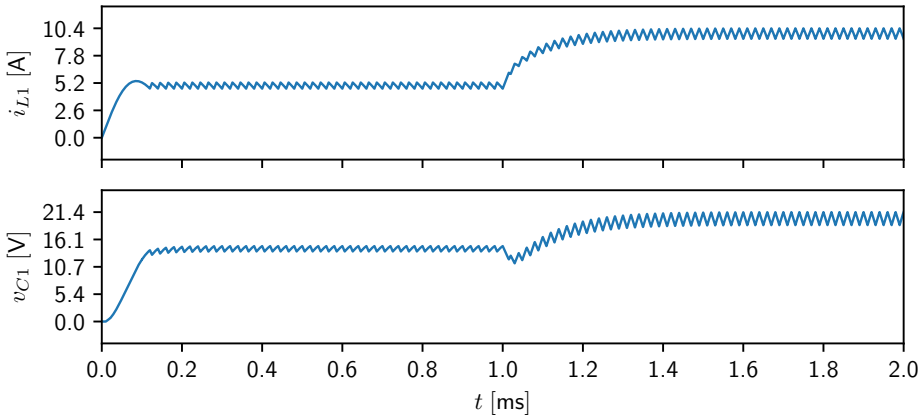


FIGURE 5 Boost converter's transient response with applied NMPC with prediction horizon $N = 2$ in the case when duty-ratio changes from the value $\overline{d} = 0.3$ to $\overline{d} = 0.5$ after $t = 1$ ms from startup.

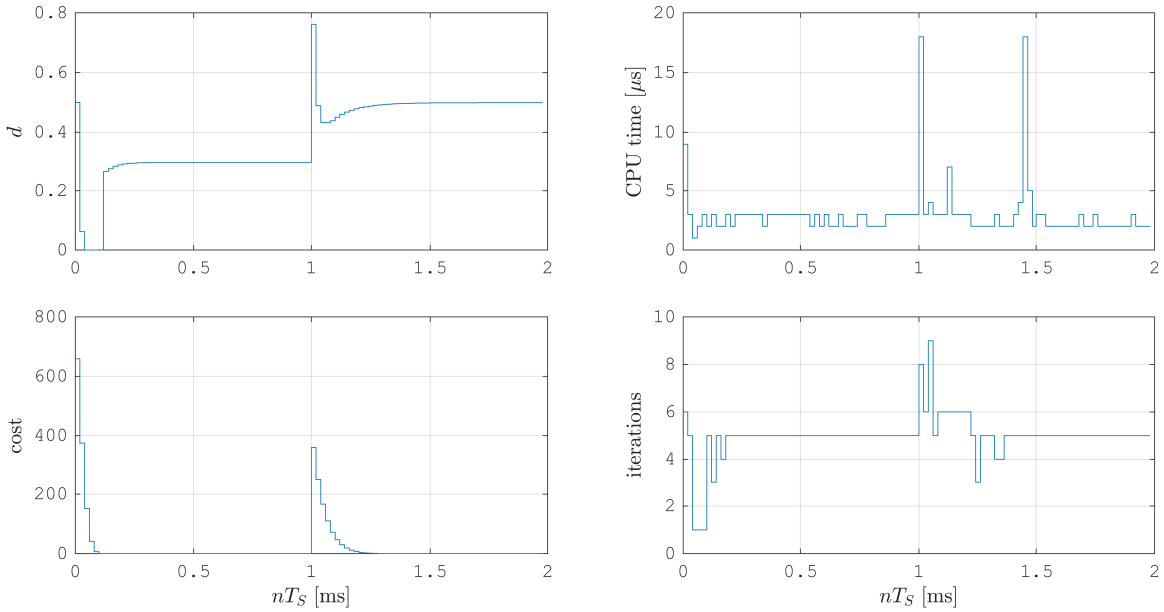


FIGURE 6 Optimal duty ratios, objective function values, CPU times and PANOC iterations for NMPC with a horizon $N = 2$ in case the duty-ratio of the boost converter changes from $\overline{d} = 0.3$ to $\overline{d} = 0.5$ after $t = 1$ ms from startup.

In the second example, a constant desired duty-ratio $\overline{d} = 0.3$ is maintained, but the input voltage changes from $v_{IN} = 10$ V to $v_{IN} = 20$ V after 1 ms. Figure 7 presents the transient diagrams of the state variables for this case of changing the desired operating point from $\overline{x} = [5.1\text{ A},\ 14.29\text{ V}]^\intercal$ to $\overline{x} = [10.2041\text{ A},\ 28.5714\text{ V}]^\intercal$ after 1 ms caused by the input voltage change. Figure 8 provides results of running the simulation with optimal duty ratios, objective function values, CPU times and PANOC iterations. Again, it can be concluded that even in the case of the change in the operating condition, the CPU time is shorter than the switching period.

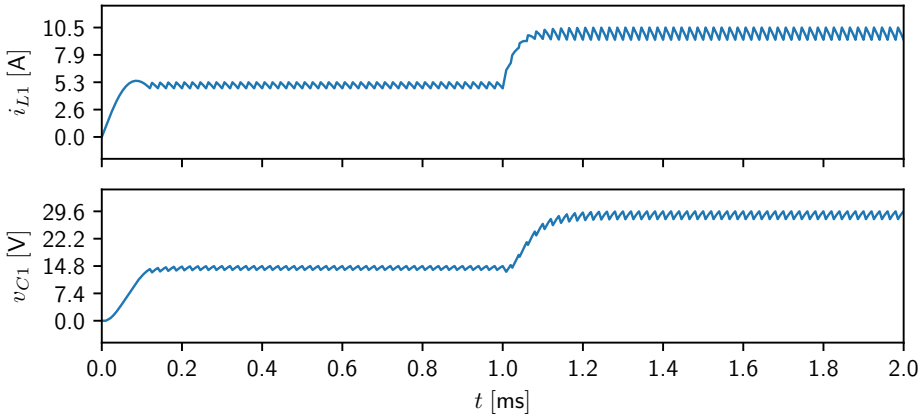


FIGURE 7 Boost converter's transient response with applied NMPC with prediction horizon $N = 2$ in the case when input voltage changes from the value $v_{IN} = 10$ V to $v_{IN} = 20$ V after $t = 1$ ms from startup.

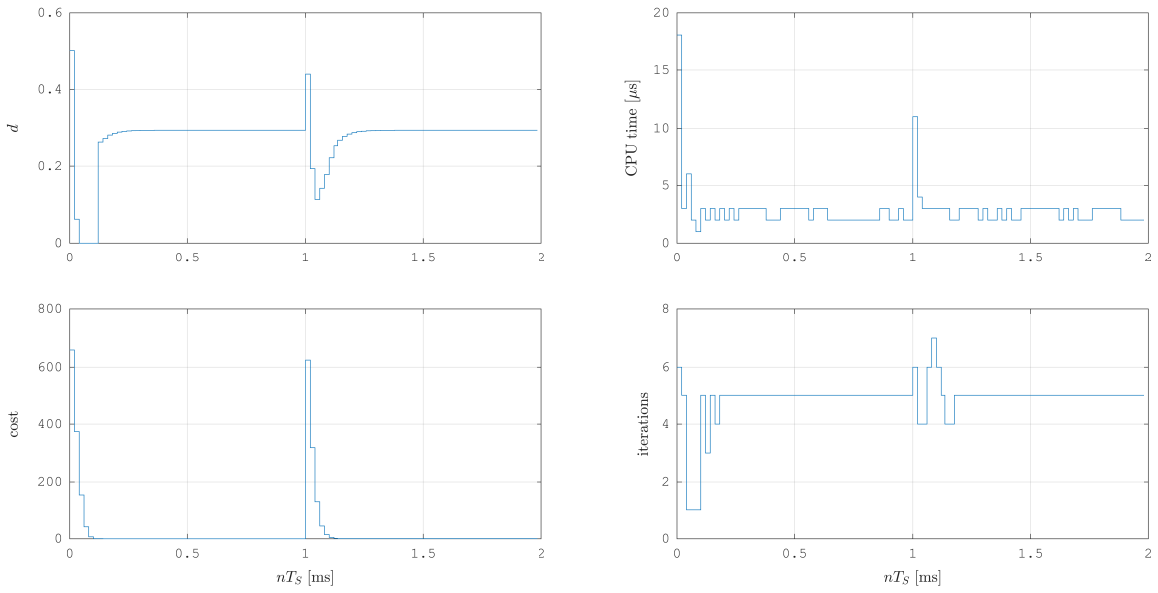
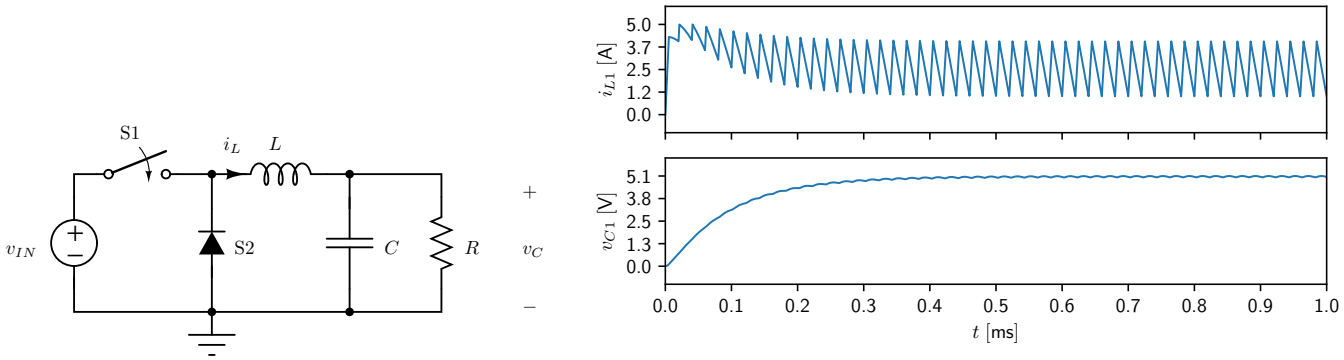


FIGURE 8 Optimal duty ratios, objective function values, CPU times and PANOC iterations for the resulting optimal control problem in NMPC with a horizon $N = 2$ of the boost converter in the case when duty-ratio changes from the value $v_{IN} = 10$ V to $v_{IN} = 20$ V after $t = 1$ ms from startup.

3.2 | Application of NMPC to Different Converter Topologies

Since the NMPC algorithm proposed in this paper can be applied to different converter specifications without any change in the proposed methodology, we give in this subsection simulation results for two more converter topologies: a buck converter as the other example of the standard converter topology and a Ćuk converter, which represents a complex two switch converter.

A Buck converter, depicted in Figure 9a, is simulated with the circuit parameters: $v_{IN} = 20$ V, $L = 25\,\mu$H, $C = 100\,\mu$F and $R = 2\,\Omega$. The switching frequency is again $f_S = 50$ kHz. The reference duty-ratio is $\overline{d} = 0.25$, for which the corresponding steady-state and the ripple are: $\overline{\mathbf{x}} = [\overline{i_L}\ \overline{v_C}]^\intercal = \left[\frac{\overline{d}v_{IN}}{R},\ \overline{d}v_{IN}\right]^\intercal = [2.5\text{ A},\ 5\text{ V}]^\intercal$ and $\Delta\mathbf{x} = [1.5\text{ A},\ -1.8\cdot 10^{-17}\text{ V}]^\intercal$. For the same



(a) (b)

FIGURE 9 (a) Buck converter; (b) Buck converter's transient response with NMPC applied for prediction horizon $N = 2$.

matrices Q and R, the terminal cost is

$$P = \begin{bmatrix} 1.0 & 0.17 \\ 0.17 & 4.33 \end{bmatrix}.$$

As can be seen from Figure 9b, the system is stable around desired steady-state.

In addition, an example of a Ćuk converter is considered. A Ćuk converter, depicted in Figure 10a, presents one of the most complex converters with two switches. The selected circuit parameters are: $v_{IN} = 5$ V, $L_1 = 645.4\,\mu$H, $L_2 = 996.3\,\mu$H, $C_1 = 217$ nF, $C_2 = 14.085\,\mu$F and $R = 43\,\Omega$. The control is constructed for the desired duty-ratio $\overline{d} = 0.5$ and the switching frequency $f_S = 50$ kHz. The desired steady-state value is $\overline{\mathbf{x}} = \left[\frac{\overline{d}^2}{(1-\overline{d})^2}\frac{v_{IN}}{R},\ -\frac{\overline{d}}{1-\overline{d}}\frac{v_{IN}}{R},\ \frac{v_{IN}}{1-\overline{d}},\ -\frac{\overline{d}}{1-\overline{d}}v_{IN}\right]^\intercal = [0.11627907\text{ A},\ -0.11627907\text{ A}, 10\text{ V}, -5\text{ V}]^\intercal$ and the ripple $[38.7\text{ mA}, -25.09\text{ mA}, -2.68\text{ V}, -1.76\cdot 10^{-15}\text{ V}]$. The terminal cost matrix is obtained from Eq. (16) for $Q = I_{4\times 4}$ and $R = 0.1$, as

$$P = \begin{bmatrix} 3055.93 & 1257.74 & 13.55 & -32.66 \\ 1257.74 & 551.33 & 4.95 & -2.08 \\ 13.55 & 4.95 & 1.07 & -0.36 \\ -32.66 & -2.08 & -0.36 & 5.99 \end{bmatrix}.$$

Figure 10b shows that the proposed NMPC scheme successfully stabilizes the Ćuk converter, which is not easily obtained by standard PID controllers. The converter reaches its steady-state with a minimal "overshoot", using NMPC with the reduced prediction horizon $N = 2$. The "overshoot" is minimal taking into the account that this converter operates only between marginally stable subsystems in the continuous conduction mode, and thus, it is not easily stabilizable converter.

4 | EXPERIMENTAL RESULTS

DSpace MicroLabBox with its 2 GHz CPU speed and with 1 GB RAM memory is a commonly used system for the implementation of MPC algorithms and generally for the easy implementation of high demanding switching control. MicroLabBox is

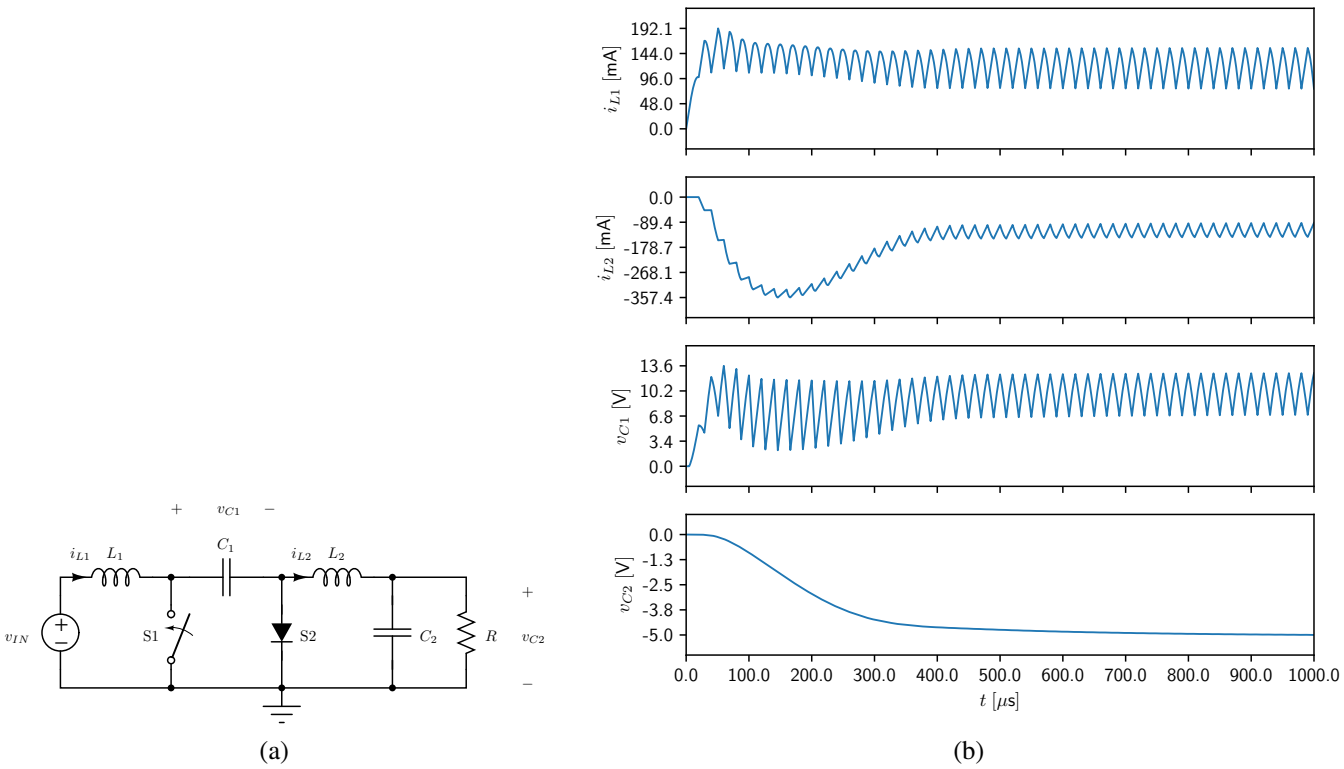


FIGURE 10 (a) Ćuk converter; (b) Ćuk converter's transient response with NMPC applied for prediction horizon $N = 2$.

also a very expensive solution that would ensure the implementation of the presented NMPC algorithm preserves its computational speed. However, since the purpose of this section is to demonstrate the NMPC algorithm, we have used instead publicly available hardware, a cheap general purpose Cortex-M7 microcontroller STM32F746 running on a frequency of 216 MHz and a MEANWELL RS-15-3.3 input voltage source generating 3.3 V and a maximum power of 15 W.

Using these components increased the computational time of the algorithm in the experiment up to around 500 μs. Thus, we have constructed a boost converter that operates with the switching frequency of 1 kHz, so the algorithm could be successfully run with the available hardware. The other circuit components are $L_1 = 1.1$ mH, $C_1 = 1$ mF, $R = 4.7\,\Omega$, a transistor IRF530 and a diode 1N5822. For the purpose of the control implementation, the inductor current is measured on the shunt resistor with $r_s = 0.1\,\Omega$ added in series with the inductor. Adding of the shunt resistor and of the real switches introduces losses in the system matrices, resulting in:

$$A_0 = \begin{bmatrix} -\frac{r_s+r_t}{L_1} & 0 \\ 0 & -\frac{1}{RC_1} \end{bmatrix}, \; b_0 = \begin{bmatrix} \frac{v_{IN}-V_t}{L_1} \\ 0 \end{bmatrix},$$
$$A_1 = \begin{bmatrix} -\frac{r_s+r_d}{L_1} & -\frac{v_C}{L_1} \\ \frac{1}{C_1} & -\frac{1}{RC_1} \end{bmatrix}, \; b_1 = \begin{bmatrix} \frac{v_{IN}-V_d}{L_1} \\ 0 \end{bmatrix}, \tag{22}$$

where V_t and r_t present the estimated Thevenin equivalent of the conducting transistor, and V_d and r_d the Thevenin equivalent of the conducting diode. After consulting the datasheets for the used diode and transistor, the values are estimated to be $V_t = V_s = 0.6$ V and $r_t = r_d = 0.16\,\Omega$.

In order to implement the experiment, the inductor current, capacitor voltage and input voltage are transformed to the voltages in the range from 0 V to 3.3 V using active and passive components, measured using ADC peripheral integrated into the microcontroller, and scaled in the software to actual values. Measured current and voltages are further used to estimate the optimal duty-ratio, which is used to update output PWM "online". Estimation of the optimal duty-ratio is completely implemented using the simulator generated C files. Besides the control algorithm and associated ADC and timer routines, the microcontroller runs a background serial communication process which is used to send the measured currents and voltages and calculated duty-cycles to the remote computer. Software running on the computer is used to collect, visualize and save the data in the log file,

which is used for further analysis and plotting. The data is measured twice per switching period, at the rising and falling edge of the output PWM. The data measured at the rising edge are used in the control algorithm to set the duty-cycle of the PWM in the next switching period. The data measured at both the rising and falling edge are sent to the computer.

For the desired duty-ratio $d = 0.4$, the calculated steady-state is $\overline{x} = [1.38\ \text{A},\ 3.9\ \text{V}]^\intercal$. This case is simulated using the NMPC simulator and depicted in the Figure 11, showing the expected operation of the constructed boost converter with NMPC applied.

To verify operation of the simulator and the controlling method itself, the same diagrams obtained experimentally are given in Figure 12. The diagrams are plotted using the data measured by microcontroller twice per switching period, triggered on the PWM rising edge and on the PWM falling edge. It is important to note that the values shown in Fig. 12 at the switching instances are real, and the data between them are linearly interpolated. In order to demonstrate that the boost converter reaches its steady-state operation, oscilloscope steady-state diagrams are provided in Figure 13.

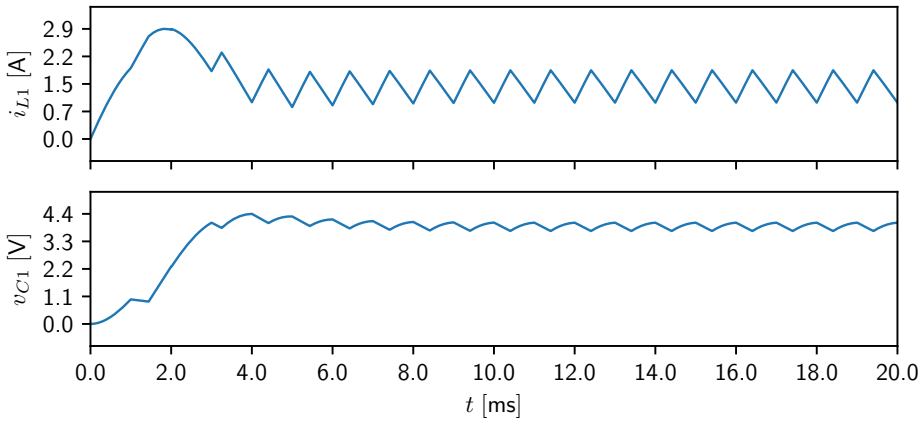


FIGURE 11 Simulated startup transient waveforms of the constructed boost converter.

5 | CONCLUSION

In this paper we presented an NMPC algorithm for DC-DC converters operating in CCM. The algorithm is implemented and incorporated inside the simulator for DC-DC converters, which can be downloaded from the repository [25]. Solving the resulting optimal control problem relies on the PANOC method, which exhibits very fast convergence behavior. The developed NMPC algorithm for DC-DC converters is stable and provides the desired response without overshoot in the transient diagrams of the state variables. In order to demonstrate the simulator's operation, simulation of the boost converter in the open loop and with PID-controller is compared to the diagrams generated using NMPC. The generated diagrams show that the NMPC controlled converter converges to steady-state much faster and without overshoot during its transient. The experimental implementation proved that the algorithm is implementable and relatively fast. Though achieving switching frequencies of order of tens of kHz would require a significantly faster general purpose scalar processor, a parallel FPGA or ASIC implementations could always be a solution. Furthermore, to the best of the authors' knowledge, this is still the only "online" implementation of an adaptive control algorithm with this performance.

ACKNOWLEDGEMENTS

A. Lekić's research visit at KU Leuven has been supported by Coimbra Scholarship Programme for Young Researchers from the European Neighbourhood in 2018. This work was also supported by FWO projects: G086318N; G086518N; Fonds de la Recherche Scientifique - FNRS and the Fonds Wetenschappelijk Onderzoek - Vlaanderen under EOS Project no 30468160 (SeLMA). B. Hermans' work benefits from KU Leuven-BOF PFV/10/002 Centre of Excellence: Optimization in Engineering

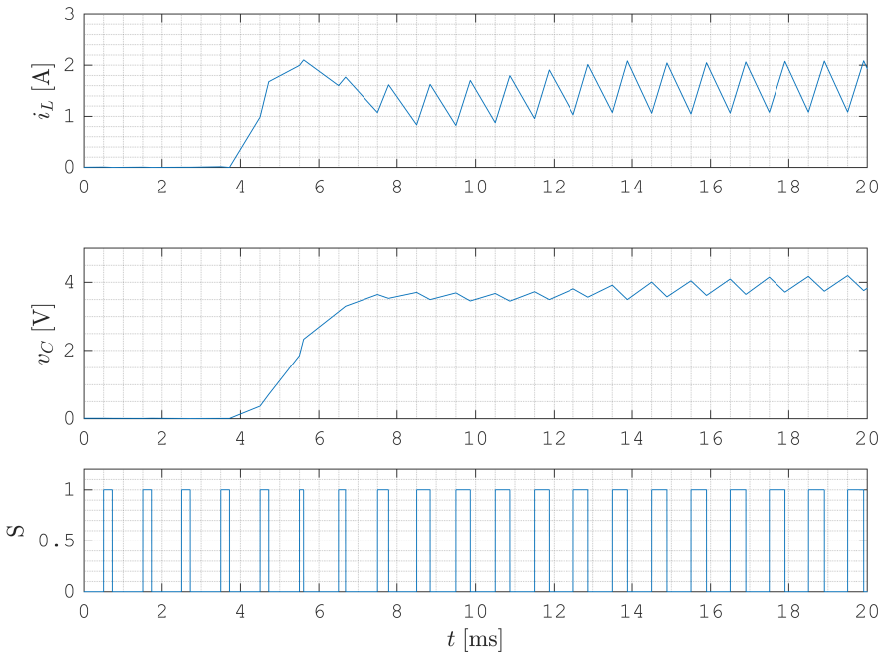
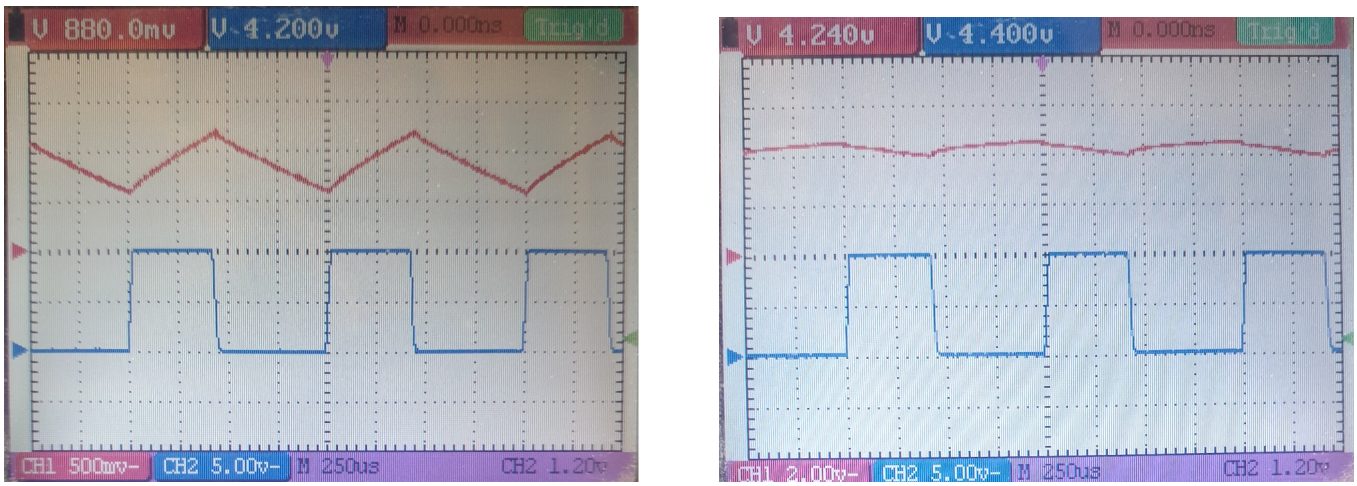


FIGURE 12 Experimentally obtained diagrams for inductor current, capacitor voltage and generated PWM signal.



(a) (b)

FIGURE 13 Experimentally obtained steady-state waveforms for: (a) CH1 - inductor current and CH2 - generated PWM signal; (b) CH1 - capacitor voltage and CH2 - generated PWM signal.

(OPTEC), from project G0C4515N of the Research Foundation - Flanders (FWO - Flanders), from Flanders Make ICON: Avoidance of collisions and obstacles in narrow lanes, and from the KU Leuven Research project C14/15/067: B-spline based certificates of positivity with applications in engineering.

References

1. Erickson RW, Maksimovic D. *Fundamentals of power electronics*. Springer Science & Business Media . 2001.
2. Al-Turki Y, El Aroudi A, Mandal K, et al. Nonaveraged control-oriented modeling and relative stability analysis of DC-DC switching converters. *International Journal of Circuit Theory and Applications* 2018; 46(3): 565–580.
3. Giaouris D, Maity S, Banerjee S, Pickert V, Zahawi B. Application of Filippov method for the analysis of subharmonic instability in dc–dc converters. *International Journal of Circuit Theory and Applications* 2009; 37(8): 899–919.
4. Liu GP. Predictive controller design of networked systems with communication delays and data loss. *IEEE Transactions on Circuits and Systems II: Express Briefs* 2010; 57(6): 481–485.
5. Yang J, Zheng WX. Offset-free nonlinear MPC for mismatched disturbance attenuation with application to a static var compensator. *IEEE Transactions on Circuits and Systems II: Express Briefs* 2014; 61(1): 49–53.
6. Ong CJ, Wang Z, Dehghan M. Model predictive control for switching systems with dwell-time restriction. *IEEE Transactions on Automatic Control* 2016; 61(12): 4189–4195.
7. Zhang L, Zhuang S, Braatz RD. Switched model predictive control of switched linear systems: Feasibility, stability and robustness. *Automatica* 2016; 67: 8–21.
8. Geyer T, Papafotiou G, Morari M. Hybrid model predictive control of the step-down DC–DC converter. *IEEE Transactions on Control Systems Technology* 2008; 16(6): 1112–1124.
9. Beccuti AG, Mariéthoz S, Cliquennois S, Wang S, Morari M. Explicit model predictive control of DC-DC switched-mode power supplies with extended Kalman filtering. *IEEE Transactions Industrial Electronics* 2009; 56(6): 1864–1874.
10. Kouro S, Cortés P, Vargas R, Ammann U, Rodríguez J. Model predictive control–A simple and powerful method to control power converters. *IEEE Transactions on Industrial Electronics* 2009; 56(6): 1826–1838.
11. Aguilera RP, Lezana P, Quevedo DE. Switched model predictive control for improved transient and steady-state performance. *IEEE Transactions on Industrial Informatics* 2015; 11(4): 968–977.
12. Oettmeier FM, Neely J, Pekarek S, DeCarlo R, Uthaichana K. MPC of switching in a boost converter using a hybrid state model with a sliding mode observer. *IEEE Transactions Industrial Electronics* 2009; 56(9): 3453–3466.
13. Karamanakos P, Geyer T, Manias S. Direct model predictive current control strategy of DC–DC boost converters. *IEEE Journal of Emerging and Selected Topics in Power Electronics* 2013; 1(4): 337–346.
14. Cavanini L, Cimini G, Ippoliti G, Bemporad A. Model predictive control for pre-compensated voltage mode controlled DC–DC converters. *IET Control Theory & Applications* 2017; 11(15): 2514–2520.
15. Cheng L, Acuna P, Aguilera RP, et al. Model Predictive Control for DC–DC Boost Converters With Reduced-Prediction Horizon and Constant Switching Frequency. *IEEE Transactions on Power Electronics* 2018; 33(10).
16. Yfoulis C. An MPC Reference Governor Approach for Enhancing the Performance of Precompensated Boost DC–DC Converters. *Energies* 2019; 12(3): 563.
17. Uno M, Igarashi R, Sato Y. Switched Capacitor Converter-Based PWM Plus Phase-Shift Control Multiport Converter with Differential Power Processing Capability for Photovoltaic Systems. In: IEEE. ; 2019: 1–8.
18. Novak M, Nyman UM, Dragicevic T, Blaabjerg F. Analytical design and performance validation of finite set MPC regulated power converters. *IEEE Transactions on Industrial Electronics* 2018; 66(3): 2004–2014.
19. Rodriguez J, Kazmierkowski MP, Espinoza JR, et al. State of the art of finite control set model predictive control in power electronics. *IEEE Transactions on Industrial Informatics* 2012; 9(2): 1003–1016.
20. Richter S, Mariéthoz S, Morari M. High-speed online MPC based on a fast gradient method applied to power converter control. In: IEEE. ; 2010: 4737–4743.

21. Kouro S, Cortés P, Vargas R, Ammann U, Rodríguez J. Model predictive controlâĂŤA simple and powerful method to control power converters. *IEEE Transactions on industrial electronics* 2008; 56(6): 1826–1838.

22. Rossi M, Piegari L, Castelli-Dezza F, Mauri M, Carmeli MS. Voltage Control Comparison for Low-Power DC-DC Converters in EVs: PI and Explicit MPC. In: IEEE. ; 2018: 5005–5011.

23. Melis W. NMPC-codegen. https://github.com/kul-forbes/nmpc-codegen; 2018.

24. Lekić A. Simulation of PWM DC-DC converters using eigenvalues and eigenvectors. *Journal of Electrical Engineering* 2017; 68(1): 13–22.

25. Lekić A. DC–DC simulator. https://github.com/kul-forbes/dc_dc_simulator; 2019.

26. Stella L, Themelis A, Sopasakis P, Patrinos P. A simple and efficient algorithm for nonlinear model predictive control. In: IEEE. ; 2017: 1939–1944.

27. Andersson JA, Gillis J, Horn G, Rawlings JB, Diehl M. CasADi: a software framework for nonlinear optimization and optimal control. *Mathematical Programming Computation* 2018: 1–36.

28. Khalil HK. Noninear systems. *Prentice-Hall, New Jersey* 1996; 2(5): 5–1.

29. Rawlings J, Mayne D, Diehl M. *Model Predictive Control: Theory, Computation, and Design*. Nob Hill Pub. Madison, Wisconsin . 2018.

30. Aguilera RP, Quevedo DE, others . On stability and performance of finite control set MPC for power converters. In: IEEE. ; 2011: 55–62.

31. Limon D, Alamo T, Camacho E. Stable constrained MPC without terminal constraint. In: . 6. IEEE. ; 2003: 4893–4898.

32. Yfoulis C, Giaouris D, Ziogou C, Stergiopoulos F, Voutetakis S, Papadopoulou S. Optimal switching Lyapunov-based control of power electronic converters. *International Journal of Circuit Theory and Applications* 2017; 45(3): 354–375.

33. Egerstedt M, Wardi Y, Delmotte F. Optimal control of switching times in switched dynamical systems. In: . 3. IEEE. ; 2003: 2138–2143.

34. Kawashima H, Wardi Y, Taylor D, Egerstedt M. Optimal switching control of a step-down DC-DC converter. In: IEEE. ; 2012: 1454–1459.

35. Lekić A. Automated DC-DC converters symbolic state-space model generation by the use of free software. In: IEEE. ; 2014: 995–998.

36. Yousefzadeh V, Babazadeh A, Ramachandran B, Alarcón E, Pao L, Maksimovic D. Proximate time-optimal digital control for synchronous buck DC–DC converters. *IEEE Transactions on Power Electronics* 2008; 23(4): 2018–2026.

How to cite this article: A. Lekić, B. Hermans, P. Patrinos and N. Jovičić (2019), Microsecond Nonlinear Model Predictive Control for DC-DC Converters, *Int J Circ Theor Appl*